Spectral tuning and emission enhancement through lanthanide coordination in a dual Vis-NIR emissive cyanide-bridged heterometallic Ru(II)-Er(III) complex

Journal:	*Crystal Growth & Design*
Manuscript ID	cg-2024-00115j
Manuscript Type:	Article
Date Submitted by the Author:	25-Jan-2024
Complete List of Authors:	Mara, Dimitrije; Università degli Studi del Piemonte Orientale Amedeo Avogadro, Dipartimento per lo Sviluppo Sostenibile e la Transizione Ecologica (DiSSTE) Cai, Zhiwang; Ghent University, Department of Chemistry Bonabello, Silvia; Università degli Studi del Piemonte Orientale Amedeo Avogadro, Dipartimento per lo Sviluppo Sostenibile e la Transizione Ecologica (DiSSTE) Penna, Stefano; Thales Alenia Space Italia, Chief Technical Office Van Deun, Rik; Universiteit Gent, Department of Inorganic and Physical Chemistry Deplano, Paola; Università di Cagliari , Dipartimento di Ingegneria Civile, Ambientale e Architettura Marchiò, Luciano; Universita degli Studi di Parma, Department of Chemistry, Life Sciences and Environmental Sustainability Pilia, Luca; Universita degli Studi di Cagliari, Dipartimento di Ingegneria Meccanica, Chimica e dei Materiali Artizzu, Flavia; University of Eastern Piedmont, Department of Sustainable Development and Ecological Transition (DISSTE)

Spectral tuning and emission enhancement through lanthanide coordination in a dual Vis-NIR emissive cyanide-bridged heterometallic Ru(II)-Er(III) complex

Dimitrije Mara[a], Zhiwang Cai[b], Silvia Bonabello[a], Stefano Penna[c], Rik Van Deun[b], Paola Deplano[d], Luciano Marchiò[e], Luca Pilia,[f,] and Flavia Artizzu[a,*]*

[a] Dipartimento per lo Sviluppo Sostenibile e la Transizione Ecologica (DiSSTE), Università del Piemonte Orientale "A. Avogadro", Piazza S. Eusebio 5, 13100 Vercelli, Italy

[b] L^3 - Luminescent Lanthanide Lab, Department of Chemistry, Faculty of Sciences, Ghent University, Krijgslaan 281, S3, B-9000 Ghent, Belgium

[c] Thales Alenia Space Italia, Chief Technical Office, via Saccomuro 24, 00131 Roma, Italy

[d]Dipartimento di Ingegneria Civile, Ambientale e Architettura, Università di Cagliari, Via Marengo 2, 09123 Cagliari, Italy

[e] Dipartimento di Scienze Chimiche, della Vita e della Sostenibilità Ambientale, Università di Parma, Parco Area delle Scienze 17/a, 43124 Parma, Italy

[f] Dipartimento di Ingegneria Meccanica Chimica e dei Materiali, Università di Cagliari, Via Marengo 2,09123 Cagliari, Italy

KEYWORDS Ru(II) complexes; erbium emission; d-f assemblies; luminescence quantum yield.

GRAPHICAL ABSTRACT

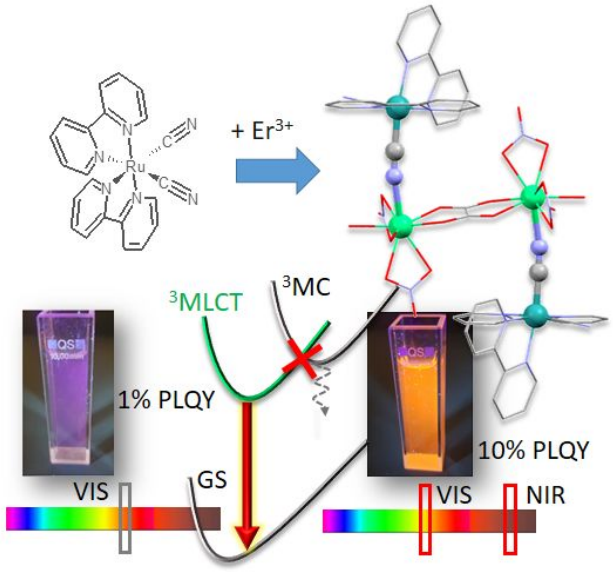

ABSTRACT

Owing to their unique luminescent properties and photosensitizing capability, cyanoruthenium(II) complexes with diimine ligands are the subject of intense research striving for routes for tuning their electronic properties and improving their emission quantum yield. In this work, we describe the first example of a heterometallic *d-f* cyanide-bridged Ru(II)-Er(III) assembly obtained by the direct reaction of trivalent erbium salt with the neutral $[Ru(bipy)_2(CN)_2]$ metalloligand. This strategy allows for accommodating inorganic negatively charged anions, such as nitrate and oxalate, in the coordination sphere of the lanthanide ion. As a result, a dimeric tetranuclear discrete molecular architecture is obtained, where the two constituting monomeric Ru(II)-CN-Er(III) units are bridged by an oxalate anion coordinating two Er(III) ions in a bis-bidentate fashion. Strikingly, this heterometallic compound shows intense dual emission in the visible and near-infrared spectral ranges under single-wavelength excitation both in solution and in the crystalline state. The effect of Er(III) coordination through a cyanide bridge is thoroughly discussed, also with the support of DFT calculations, to highlight the factors that induce the observed spectral hypsochromism and, more importantly, the remarkable tenfold-increased emission quantum yield of the $[Ru(bipy)_2(CN)_2]$ moiety in the visible range. We show that the described coordination mode

induces an energy raise of the emissive ^{3}MLCT state and even a more pronounced lifting of the non-emissive Ru(II) ^{3}MC states, suppressing thermal deactivation channels. Furthermore, thanks to the reduced number of water molecules and quenching groups surrounding the lanthanide ion in the molecular architecture, relatively intense erbium emission at 1.5 μm telecom wavelength is detected through the sensitization from the Ru(II) metalloligand. We suggest that this compound can find applications as efficient solid-state dual emitter and luminescent chemical sensor.

1. INTRODUCTION

Ru(II) polypyridine complexes have been the subject of great attention because of the remarkable optical and redox properties enabling applications in a wide range of different fields including photocatalysis[1], luminescent chemical sensing[2]-, solar cells[3] and anticancer drugs[4]. The unique photochemical and photophysical properties of Ru(II) complexes stem from the activation of triplet metal-to-ligand charge-transfer (^{3}MLCT) excited states which are long-lived, characterized by a broad emission profile, and are susceptible to give rise to both photoinduced energy or electron transfer to a secondary species allowing it to reach states otherwise poorly accessible under direct excitation[5]. Therefore, extensive research has been performed in the last three to four decades on the tuning of the energy levels and the optical properties of Ru(II) complexes with the

aim of improving the photosensitizing properties and the emission quantum yield[6]. Among the class of luminescent Ru(II) diimine complexes, heteroleptic cyanoruthenate derivatives are of particular interest because of the striking sensitivity to the chemical environment, making them suitable visual chemical sensors both in absorption and emission[7,8,9]. Moreover, thanks to the lone pair borne by the nitrogen atom, cyanide groups are highly suitable to form stable cyanide-bridged M−CN−M' heterometallic complexes with a simple click chemistry[10,11,12]following the complex-as-ligand approach. This allows for the introduction of novel functionalities either magnetic or optical properties[13], opening novel perspectives for the applications of such molecular architectures. With this view, Ru(II) complexes with cyanide ligands have been explored as ideal molecular photosensitizers of luminescent trivalent lanthanide (Ln) ions, where the short cyanide bridge allows for a limited Ru-Ln distance, in principle a favorable requisite for efficient donor-acceptor Förster's energy transfer and subsequent Ln photosensitization[10,12]. Moreover, bridging cyanide groups act as spacers between the emitting Ln(III) center and the peripheral organic chromophoric ligands of the *d*-metal moiety, thus limiting the distance-dependent vibrational quenching related to CH oscillators[14]. These properties have been so far relatively investigated only in heterometallic *d-f* derivatives of the negatively charged tetracyanoruthenate(II) complex

$[Ru(L)(CN_4)]^{2-}$ (L = diimine ligand), which have also found applications as chemodosimeters through an indicator displacement assay approach[15,16]. In the available literature examples, the direct reaction of $[Ru(L)(CN)_4]^{2-}$ with trivalent Ln cations afford an extremely rich and complex structural chemistry, owing to the availability of four CN^- groups, comprising 1D to 3D polymers and oligomers. As a consequence of the monodentate binding mode of cyanide groups and the high coordination numbers of Ln ions, several water molecules, which are the most severe quenchers of Ln luminescence, remain coordinated to the Ln center[17]. On the other hand, it has been demonstrated that a blocking ligand coordinated to the Ln ion is beneficial to their luminescence, reducing the available coordination sites for water molecules[18]. Following these concepts, we envisaged that using the neutral *cis*-dicyano-bis (2,2'-bipyridine) ruthenium(II) $[Ru(bipy)_2(CN)_2]$ complex instead of the doubly negatively charged tetracyano analog, allows for completing the coordination sphere of Ln ions with quenchers-free inorganic anions such as nitrate and oxalate. In this work, we report the synthesis, structure and the photophysical properties of a tetranuclear Ru(III)-Er(III) mixed metal complex, which, to the best of our knowledge, represents the first example of a *d-f* architecture with the $[Ru(L)_2(CN)_2]$ building block. We show that the heterometallic compound displays dual emission in the visible and in the near-infrared (NIR)

spectral range owing to the $[Ru(bipy)_2(CN)_2]$ metal-to-ligand charge transfer (^{3}MLCT) and Er(III) centered luminescence at 1.53 μm, an important wavelength for telecommunication technology. Strikingly, we found that, upon coordination to Er(III), the emission of $[Ru(bipy)_2(CN)_2]$ not only displays a significant hypsochromic shift both in solution and in the cystalline state, but also a remarkable increased quantum yield of 10% with respect to the 0.9% of the Ru(II) precursor complex, contrary to previous literature reports on analogous compounds[1]. With the support of Density Functional Theory calculations we shed light on the structure/property relationship in such assembly, highlighting the pivotal role of cyanide groups and coordination effects on the observed properties.

2. EXPERIMENTAL SECTION

Syntheses. All reactants and solvents were purchased from Sigma-Aldrich (Sigma-Aldrich, Saint-Louis, MO, USA) or Merck (Merck KGaA, Whitehouse Station, NJ, USA) and used without further purification. *Synthesis of cis-dicyano-bis (2,2'-bipyridine) ruthenium(II) $[Ru(bipy)_2(CN)_2]$ (**Ru**).* Oxalatobis(2,2'-bipyridine)ruthenium(II) $[Ru(bipy)_2ox]$ was first synthesized according to a slight modification of the method described by Liu et al.[19] Briefly, 1.16g of the commercial potassium hexachlororuthenate(IV) salt and 1.5 g of potassium oxalate K_2ox in 40 mL of water

were heated in a steam bath for 2h. Afterwards, a solution of 0.8 g of 2,2'-bipyridine in 10 mL of methanol was added to the above mixture, which was further heated for 3h. Upon cooling, the solid product formed, which was washed several times with hot water and dried with diethyl ether. The following procedure was carried out according to the method described by Demas et al.[20] The recovered product (1.0 g) was then dissolved in 100 mL of methanol and a solution of 1.0 g of KCN in 25 mL of water was added to the mixture, which was refluxed for 48 h. The solution was then rotoevaporated to dryness and extracted twice with hot water. The solid was redissolved in methanol and crystallized by adding diethylether. Elemental analysis was in agreement with a $[Ru(bipy)_2(CN)_2]\cdot 0.5K_2ox\cdot 2H_2O$ formulation. *Elem. Anal.* Exp. (Calcd for C24H20N6KO4Ru) C% 48.40 (48.59) H% 3.75 (3.55) N% 14.65 (14.78). This formulation is also consistent with FT-IR data (Figure S2 and related discussion) *FT-IR (cm^{-1}).* 3460 mw,br; 2057 m; 1637 mw; 1469 mw; 1442 mw; 1423 w; 1388 ms; 1314 w; 1271 w; 1248 w; 1158 w;1119 vw; 772 m; 738 m; 660 w; 520 w; 415 w. *Synthesis of $[Ru_2(Bipy)_4(CN)_4Er_2(NO_3)_4(H_2O)_4(ox)]\cdot 5H_2O$ (**RuEr**).* 0.13 g of $[Ru(bipy)_2(CN)_2]$ were dissolved in 50 mL of a 4:1 mixture of acetonitrile and methanol under gentle heating. Afterwards, a solution of 0.12 g of $Er(NO_3)_3\cdot 5H_2O$ dissolved in 30 mL of acetonitrile was added and the mixture was left stirring. After 3h, orange prismatic crystals started

to form. The crystals were washed with small amounts of methanol and dried with diethylether. *Elem. Anal.* Exp. (Calcd for C46H50Er2N16O25Ru2) C% 30.12 (31.33) H% 2.99 (2.86) N% 12.55 (12.71). *FT-IR (cm^{-1}).* 3430 mw, br; 2084-2046 (split peak) m; 1637 mw, 1467 mw; 1444 mw; 1424 w; 1384 s; 1310 mw; 1274 w; 1243 w; 1158 w; 1122 w; 1070 w; 1029 w; 875 w; 839 w; 768 m; 732 mw; 527 w; 473 w; 421 w.

Analytical and spectroscopic characterization. *Elemental analysis*: Data were collected with a Carlo Erba (Carlo Erba SpA, Milano, Italia) EA1108 CHNS analyzer. *Electronic Spectroscopy UV-Vis-NIR*. Diffuse reflectance (DR) and absorption spectra in CH_3CN solution (10^{-4} mol/L) were collected with a Agilent Cary 500 spectrophotometer (Agilent Technologies, Santa Clara, CA, USA) equipped with a 150 mm diameter integrating sphere. Crystalline samples for DR spectra were dispersed on a Teflon film. *Vibrational Spectroscopy*. FT-IR spectra on KBr pellets were collected with a Bruker Equinox 55 spectrophotometer.

X-ray Crystallography. Single crystal data were collected with a Bruker D8 equipped with an APEXII area detector (Mo Kα: λ = 0.71073 Å). The intensity data were integrated from several series of exposure frames covering the sphere of reciprocal lattice[21].(Bruker (2012). APEXII. Bruker AXS Inc., Madison, Wisconsin, USA) An absorption correction was applied using the

program SADABS[22]. The structures were solved with the ShelXT[23] structure solution program using Intrinsic Phasing and refined with ShelXL[23] on F^2 with full-matrix least squares, using the Olex2 software[24]. Non-hydrogen atoms were refined with anisotropic thermal parameters. Hydrogen atoms were placed in their calculated positions.

Density Functional Theory calculations. Density Functional Theory (DFT)[25] investigations were carried out using the GAUSSIAN 16[26] software package. The functionals used throughout this study were CAM-B3LYP[27], with basis set 6-31+G(d,p)[28] for C, H, N and O atoms, and the LANL2DZ[29] and SDD[30] ECP basis sets for Ru and Er, respectively. In the case of **RuEr** all the calculations were done in single point (SP) and in gas-phase, whereas for **Ru** in addition were carried out also geometry optimizations in both gas-phase and CH_3CN; the effects of solvation were considered by the Polarizable Continuum Model. All calculations were input using atomic coordinates obtained from single X-ray data. Time-dependent DFT (TDDFT) calculations were performed in the gas-phase employing the formalism as implemented in GAUSSIAN 16[26,31,32]. TDDFT studies were done in the gas-phase for **Ru** and **RuEr** compounds and in CH_3CN for **Ru** only. The orbital isosurfaces (with isovalue plot 0.04) were visualized using ArgusLab 4.0.1[33] whereas the calculated UV-Vis electronic spectra were depicted with GaussSum software[34].

Photoluminescence measurements. Photoluminescence (PL) measurements were performed using an Edinburgh FLSP920 spectrophotometer equipped with a Hamamatsu R928P PMT detector (200–900 nm) and a Hamamatsu R5509-72 NIR PMT detector (500–1700 nm). Steady-state PL spectra were acquired using a 450 W continuous-wave (CW) xenon lamp. Appropriate

optical filters were used, and steady-state emission data were corrected for the instrumental spectral response. All PL measurements were recorded at room temperature. Solid state samples were put between quartz plates (Starna cuvettes type 20/C/Q/0.2). The internal quantum yield was measured using an integrating sphere (110 mm diameter) on the FLSP920 spectrophotometer, and white $BaSO_4$ powder was used as a reference to measure the scattered excitation light. The internal quantum yield Φ was calculated through the following equation:

$$\Phi = \frac{\varepsilon}{\alpha} = \frac{\int L_S}{\int E_R - \int E_S}$$

where ε is the number of photons emitted by the sample and α is the number of photons absorbed by the sample. L_S is the emission spectrum of the sample; E_R is the spectrum of the scattered excitation light with the $BaSO_4$ reference sample in the sphere; E_S is the spectrum of the scattered excitation light with the actual sample in the sphere.

3. RESULTS AND DISCUSSION

3.1 Synthesis and crystal structure description.

The general synthetic procedure employed to obtain the heterometallic Ru(II)-Er(III) assembly is reported in Scheme 1. The precursor *cis*-dicyano-bis (2,2'-bipyridine) ruthenium(II) $[Ru(bipy)_2(CN)_2]$ (**Ru**) complex was synthesized according to the method reported by Demas et al.[20] by reacting the oxalatobis(2,2'-bipyridine)ruthenium(II) $[Ru(bipy)_2ox]$, in turn synthesized according to Liu et al.[19], with the appropriate amount of potassium cyanide. It is worth mentioning that the synthesis of dicyanobis(diimine) ruthenium(II) complexes is often accompanied by a non-negligible amount of byproducts which demand for a number of purification steps that significantly lower the yield of the reaction. Attempts to synthesize $[Ru(bipy)_2(CN)_2]$ through the classic method by Schilt[35] did not afford a satisfactory purity. A survey of the available crystal structures on the Cambridge Crystallographic Database returned only one structure deposited[36] for $[Ru(bipy)_2(CN)_2]$, likely reflecting the difficulties in obtaining a purified crystalline product in acceptable yield. In this work, since the $[Ru(bipy)_2(CN)_2]$ complex was intended to be further reacted to produce the heterometallic complex, purification steps were reduced to avoid time-consuming procedures. The obtained product (**Ru**) was then directly reacted with the erbium nitrate salt to obtain the heterometallic complex following a similar procedure previously used to afford heterometallic Fe-Ln architectures based on the Fe(II) analog $[Fe(phen)_2CN_2]$ neutral complex[37],

where the nitrate counteranion remains coordinated to the Ln(III) metal center, serving as blocking ligand and dictating the geometry of the resulting compound. The reaction afforded crystals of the heterometallic tetranuclear $[Ru_2(bipy)_4(CN)_4Er_2(NO_3)_4(H_2O)_4(ox)]\cdot 5H_2O$ (**RuEr**) complex.

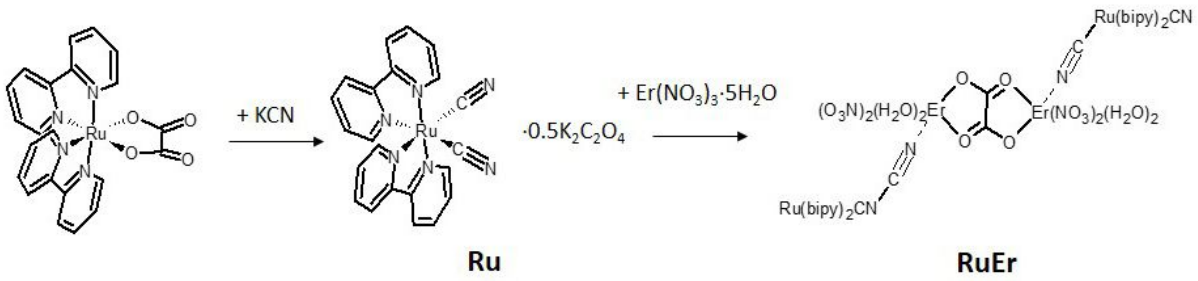

Scheme 1. General synthetic procedure for the synthesis of **RuEr**.

The molecular structure comprises a dimeric entity in which there are two peripheral Ru(II) fragments $[Ru(bipy)_2(CN)_2]$ and a central Er(III) system, namely $[Ru(bipy)_2(CN)_2]$ and $[Er_2(NO_3)_4(H_2O)_4(ox)(NC)_2]$. The connection between these entities occurs through the presence of the bridging cyanide group linking Ru(II) and Er(III) metal cations. The coordination of Ru(II) is octahedral due to the presence of two chelated bipyridine molecules and two cyanide groups in *cis* position bound via the carbon atom. The Er(III) coordination is three-capped trigonal prism, and the O_8N donor set derives from the presence of two bidentate nitrate molecules, a bidentate

oxalate molecule (bridging tetradentate on two Er(III) ions), two coordinated water molecules and a cyanide group bridging the Er(III) and Ru(II) cations, Figure 1.

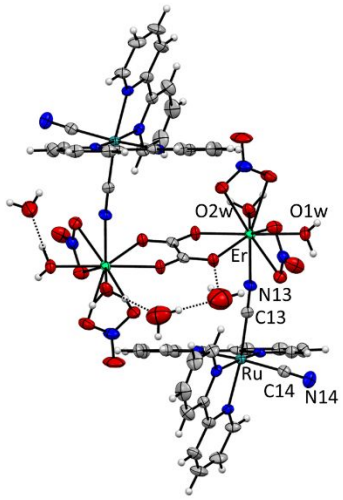

Figure 1. Molecular structure of **RuEr** with thermal ellipsoids depicted at the 30% probability level.

A summary of crystallographic parameters for **RuEr** is reported in Table 1.

Table 1. Crystallographic parameters for **RuEr**.

	RuEr
Empirical formula	$C_{46}\ H_{40}\ Er_2\ N_{16}\ O_{20}\ Ru_2 \cdot 5(H_2O)$
Formula weight	1763.68
Temperature/K	293(2)
Crystal system	triclinic
Space group	*P* -1
a, Å	11.3720(10)

b, Å	12.216(1)
c, Å	13.835(2)
α, deg.	113.363(2)
β, deg.	102.012(2)
γ, deg.	111.189(2)
V, Å^3	1500.0(4)
Z	1
ρ_{calc}g/cm^3	1.952
μ/mm^{-1}	3.358
F(000)	862.0
Crystal size/mm^3	0.11 × 0.06 × 0.04
Radiation	MoKα (λ = 0.71073)
2Θ range for data collection/°	3.516 to 51.504
Index ranges	-13 ≤ h ≤ 13, -14 ≤ k ≤ 14, -16 ≤ l ≤
Reflections collected	17185
Independent reflections	5718 [R_{int} = 0.0534, R_{sigma} =
Data/restraints/parameters	5718/2/419
Goodness-of-fit on F^2	1.020
Final R indexes [I>=2σ (I)]	R_1 = 0.0391, wR_2 = 0.0856
Final R indexes [all data]	R_1 = 0.0593, wR_2 = 0.0928
Largest diff. peak/hole / e Å^{-3}	0.88/-0.82

As described, an oxalate anion enters the coordination sphere of erbium and bridges two Er(III) ions in a bis-bidentate fashion, contributing to the significant reduction of the number of water molecules directly bonded to the lanthanide ion with respect to analog structures[17]. This oxalate molecule derives from the precursor Ru(II) complex which likely contains co-crystallized K_2ox moieties as supported by analytical data (Experimental Section) and FT-IR spectroscopy (Figure S2 and related discussion).

The dimeric entities interact with each other via a series of hydrogen bonds involving the coordination and crystallization water molecules and the nitrate anions and the terminal cyanide group. In particular, O1w behaves as an H-bond donor towards CN^- and O4w (O1w···N14 2.76 Å; O1w···O4w, 2.70 Å); O4W in turn acts as an H-bond donor towards O15 of a nitrate anion (2.98 Å). This sequence of interactions is doubled by symmetry to form a ring involving the Er^{3+} atoms. A second group of interactions involves the coordinated water molecule O2w and the O17 atom of the second nitrate anion (2.88 Å). Both sequence of interactions are doubled by symmetry and they form rings involving the Er^{3+} atoms, Figure 2a,b. In Figure 2c the crystal packing evidencing the arrangement of the dimeric entities and the water molecules of crystallization is reported.

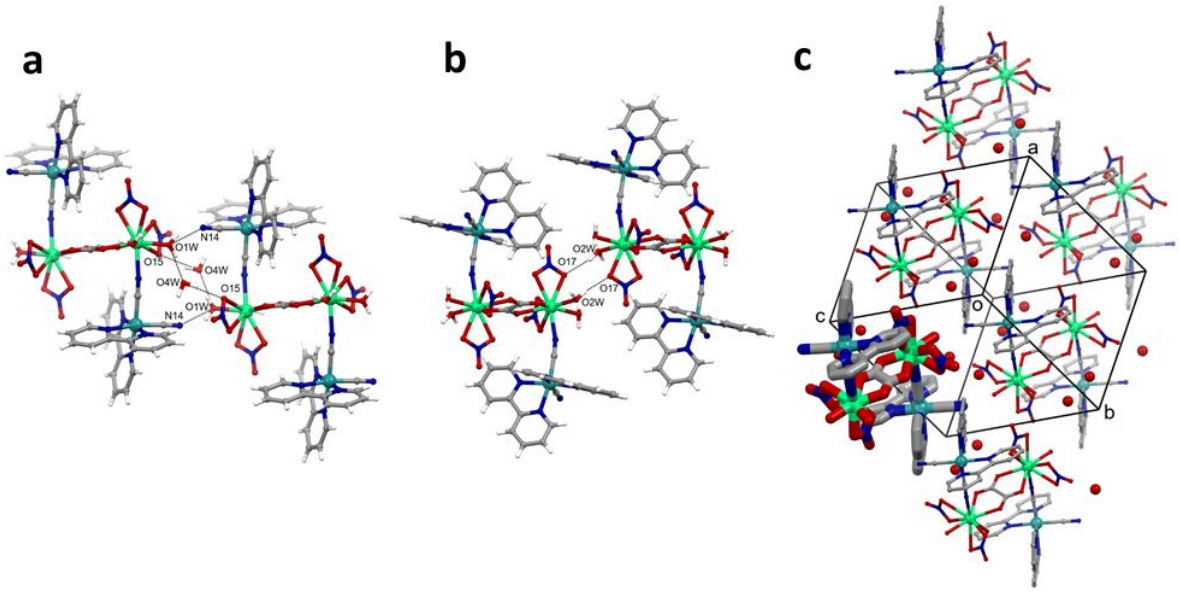

Figure 2. a, b. Highlight of the interactions occurring between symmetry related dimeric entities. c. Crystal packing of **RuEr** projected along the [111] direction. One dimeric entity is highlighted. Hydrogen atoms were omitted for clarity.

3.2 Optical Properties.

Figures 3a reports the UV-Vis optical absorption spectra of **Ru** and **RuEr** in acetonitrile solution. The spectra are characterized by a series of intense bands in the UV region and a prominent band in the visible, attributable to the $[Ru(bipy)_2(CN)_2]$ moiety in both compounds and typically assigned to ^{1}MLCT transitions as in most Ru(II) complexes[38]. This band shows a notable hypsochromism in the cyanide-bridged heterometallic **RuEr** compound with respect to the parent **Ru** complex ($\lambda_{max(\mathbf{RuEr})}$ = 450 nm *vs* $\lambda_{max(\mathbf{Ru})}$ = 494 nm), which originates from the coordination of the CN groups to the Lewis acid Er(III) ion, as also observed in analogous cyanide-bridged Fe(II)-Ln(III) assemblies[37]. Such hypsochromic shift is also evident in the diffuse reflectance spectra of solid-state samples (Figure 3b) and results in a remarkable change in color of the parent **Ru** complex upon coordination to Er(III) both in solution and in the crystalline state (Figure 3c). It is interesting to note that the solid state the spectral shape is significantly broadened (>100 nm) with respect to the solutions, as highlighted by the color differences for the two samples in the diverse phases illustrated in Figure 3c. This effect exceeds that normally expected from solid-state scattering phenomena and could be ascribed to the particularly high sensitivity of Ru(II) complexes to the chemical environment, originating from the MLCT nature of the lowest absorption band, also taking into account that numerous intermolecular interactions such as π-interactions and hydrogen bonding are present in the crystalline arrangement[39,40] (Figure S3).

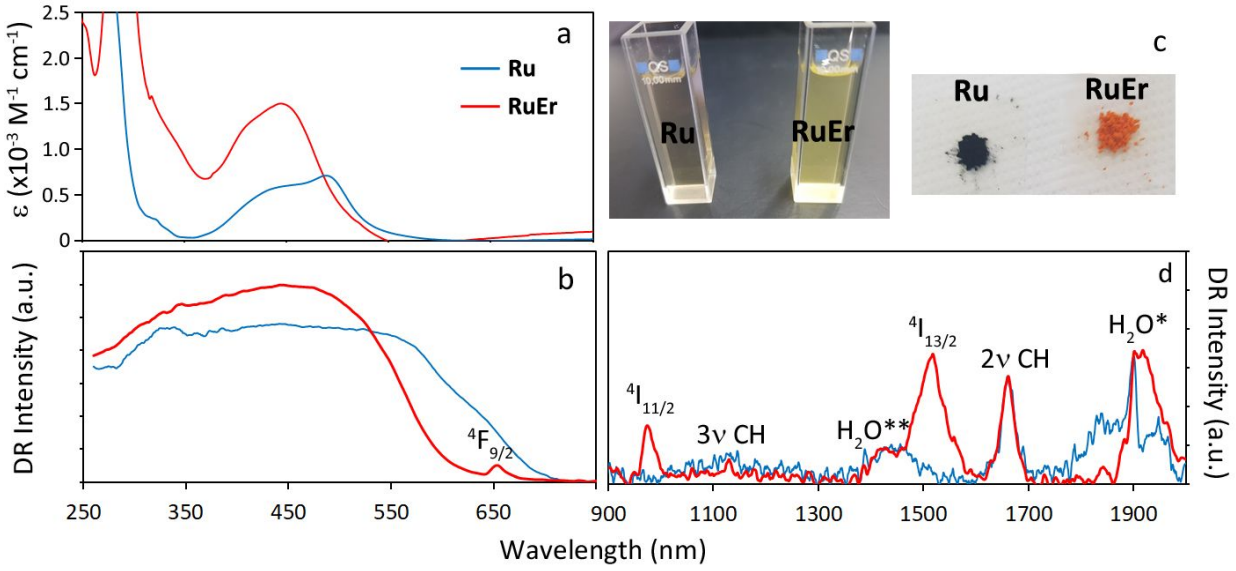

Figure 3. a) Optical absorption spectra of **Ru** (blue) and **RuEr** (red) in CH_3CN solution. b) Diffuse reflectance (DR) spectra of solid state samples in the UV-visible region. c) Pictures of CH_3CN solutions (left) and crystalline samples (right) of **Ru** and **RuEr**. d) DR spectra of solid state samples in the NIR. The Er(III) end energy levels of the transitions from the ground $^4I_{15/2}$ state are indicated. 2ν and 3ν CH indicate the second and third harmonics of CH stretching vibrations, respectively. The bands labelled H_2O* and H_2O** correspond to the $a\nu_1+\nu_2+b\nu_3$ and $\nu_1+\nu_3$ combination bands of water molecules, respectively (ν_1 = symmetric, ν_3 = antisymmetric and ν_2 = bending vibrational modes). DR spectra are normalized to the 2ν CH peak that corresponds to a single $[Ru(bipy)_2CN_2]$ moiety.

The diffuse reflectance (DR) spectrum of **RuEr** in the NIR region (Figure 3d) displays the characteristic Er(III)-centered *f-f* absorption narrow bands from the ground $^4I_{15/2}$ to the superior energy levels (978 nm $^4I_{13/2}$; 1520 nm $^4I_{13/2}$). The peaks related to the first (2ν CH, 1663 nm) and

second (3ν CH, 1132 nm) overtones of the stretching vibration of the bipy CH groups are clearly visible, as well as the H_2O combination bands at ~1920 nm (antisymmetric and symmetric stretching combination) and at ~1420 nm (stretching/bending combination). Interestingly, the H_2O stretching combination band is significantly narrower and shifted to lower energies in **RuEr** than in **Ru**, in agreement with FT-IR data (Figure S2), indicating the involvement of co-crystallized water molecules in strong hydrogen bonding, whereas these interactions are more relaxed in **Ru**. This effect reduces the spectral overlap with the erbium optical transition at 1.5 μm, with possible important implications in the NIR emission efficiency, as it will be further discussed.

3.3 Density Functional Theory calculations.

In order to reach a deeper understanding of the observed properties of **RuEr** in comparison to the precursor $[Ru(bipy)_2(CN)_2]$ complex, we performed Density Functional Theory (DFT) calculations. Figures 4a and b show the DFT-calculated Highest Occupied (HOMO) and Lowest Unoccupied (LUMO) Molecular Orbitals (MOs) of $[Ru(bipy)_2(CN)_2]$ and **RuEr**, while Tables S1-S3 report the extended set of the MOs. As it can be seen, in both compounds the HOMO is dominated by the Ru(II) *d* orbitals (t_{2g}-like orbitals in the octahedral field) with an equally relevant contribution of the π-orbitals of the CN^- groups, whereas the LUMO is largely related to

antibonding π* orbitals of the bipy ligands[41]. In **RuEr**, the coordination to the positively charged Er(III) ion induces a significant localization of the orbital density of the CN^- group on the *p* orbital of the nitrogen donor atom, likely accounting for the stabilization (Tables S1 and S3) of the mixed character Ru(II)(*d*)/CN(π) HOMO orbital, resulting in the observed hypsochromic shift of the absorption features. Since the HOMO has a significant mixed Ru(II)(*d*)/CN(π) character, the lowest absorption band in the visible range (Figures 3a and b) would therefore be better labelled as MLL'CT (metal-ligand-to-ligand charge transfer), rather than MLCT, highlighting the crucial role of the cyanide groups in determining the sensitivity of the optical (and redox[1,37]) properties to the chemical environment of cyanoruthenium(II) derivatives. It is also worth noting that in the precursor $[Ru(bipy)_2(CN)_2]$ complex, the e_g-like *d* orbitals of Ru(II) participate in the LUMO+1 (d_{z2}) and, to a less, extent, in the LUMO (d_{x2-y2}) orbitals, whereas no significant contribution of metal orbitals is observed in the first set of LUMOs in **RuEr** (Table S3).

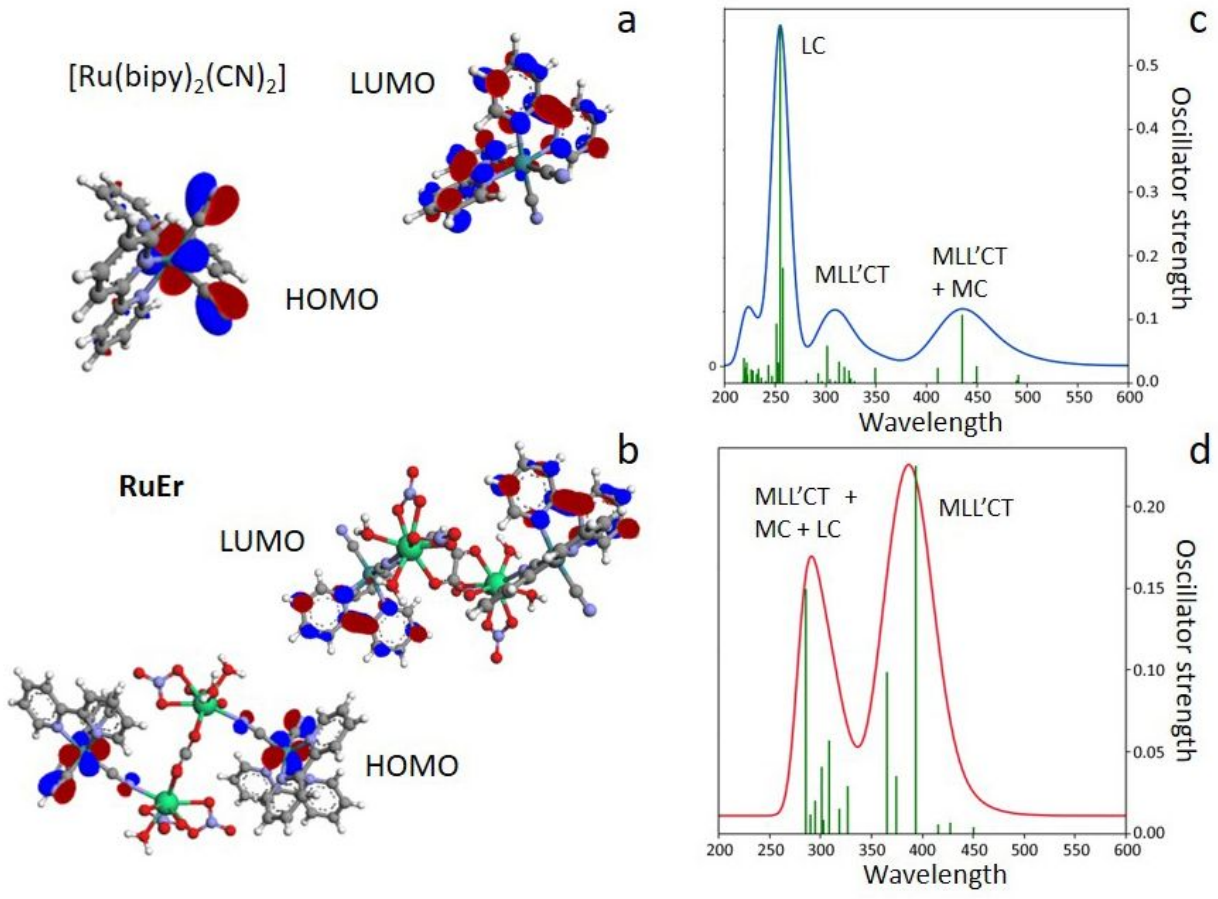

Figure 4. DFT-calculated HOMO and LUMO orbitals in the gas phase for **Ru** (a) and **RuEr** (b) and TD-DFT calculated absorption spectra for **Ru** (c) and **RuEr** (d).

Time-Dependent DFT (TD-DFT) calculations allowed to simulate the absorption spectra of the two compounds in the gas phase, as shown in Figures 4c and d. The main absorption transitions and oscillator strengths are reported in Tables S4 and S5. Although for **RuEr** the complexity of the calculations for such multiatomic assembly did not allow us to draw a complete picture of the spectrum for the first 100 states, the retrieved data provide nonetheless useful indications to

interpret the observed optical properties. As expected, calculated spectra are overall in good agreement with experimental ones confirming the observed hypsochromic shift of the lowest absorption band. In the case of $[Ru(bipy)_2(CN)_2]$, three main sets of bands can be distinguished. From the calculated main contributions of the possible transitions (Table S4) to the simulated spectral features and the orbital density distribution (Table S1), we may infer that the lowest absorption band is mainly related to MLL'CT transitions with a noticeable metal-centered (MC) contribution, as e_g-like metal orbitals are found to have a significant role in low-lying energy levels, as previously anticipated. At higher energies, the MLL'CT character becomes dominant and, on moving to the lowest wavelength part of the spectrum, the most intense band can be largely attributed to ligand-centered (LC) transitions mainly involving bipy orbitals. On the other hand, in **RuEr**, the dense set of possible transitions with comparable weight (Table S5) makes the interpretation of the nature of the spectral bands less straightforward. Nonetheless, we may reliably associate the lowest absorption band essentially to a MLL'CT character, whereas MC and LC character contributions become more relevant on going to higher energies. The main important difference that is worth highlighting in this framework between the heterometallic **RuEr** assembly

and its precursor Ru(II) complex, is the different contribution of MC-character transitions, which is a key point for the interpretation of the photoluminescence properties, as discussed further.

3.4 Photoluminescence properties.

Figure 5 summarizes the photoluminescence (PL) properties of **RuEr** compared to the precursor **Ru** complex. Upon irradiation in the absorption range, the heterometallic **RuEr** complex exhibits dual luminescence in the visible (Figures 5a, b, c) and NIR ranges (Figure 5d), related to the Ru(II) molecular unit and Er(III)-centered emission, respectively.

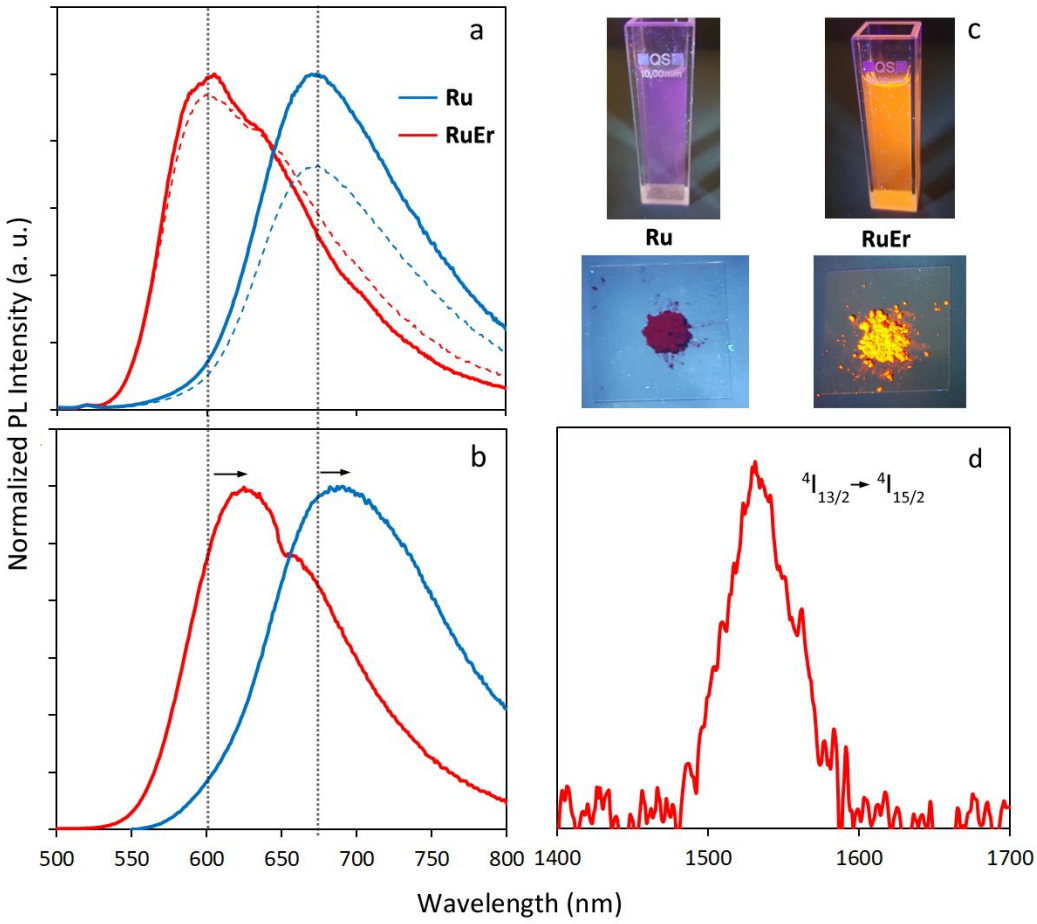

Figure 5. a) Normalized PL spectra in the visible range upon 450 nm irradiation for **RuEr** (red) and **Ru** (blue) in degassed (solid line) and air-equilibrated (dashed line) acetonitrile solution. b) Normalized PL spectra of **RuEr** (red) and **Ru** (blue) in the solid state at λ_{exc} = 450 nm. c) Photographs of **Ru** and **RuEr** in acetonitrile solution (above) and in the solid state (below) under UV (375 nm) light illumination. d) Er(III) emission spectrum for **RuEr** in the NIR range (λ_{exc} = 450 nm).

Visible range PL. The typical broad-band emission of Ru(II) polypyridine complexes, attributable to a transition from a triplet ^{3}MLCT (or ^{3}MLL'CT) state centered on the [Ru(bipy)$_2$CN$_2$] moiety, dominates in the visible range in both **Ru** and **RuEr**. However, in **RuEr**, the emission band is significantly blue-shifted with respect to the parent **Ru** complex both in acetonitrile solution (λ_{max} = 603 nm *vs* 674 nm, Figure 5a) and in the solid state (λ_{max} = 626 nm *vs* 692 nm, Figure 5b) resulting in intense orange-colored light under UV illumination as compared to the deep red light of **Ru** (Figure 5c). This effect mirrors the hypsochromic shift observed in the absorption spectra and is likewise attributed to the significant stabilization of the HOMO as a consequence of the coordination to the strong Lewis acid Er(III), as discussed above. A relatable behavior has been recently observed in analogous borylated compounds where the observed increase in energy of the ^{3}MLCT state upon the establishment of cyanide-bridges with electron-withdrawing tris(pentafluorophenyl)borane units, was correlated to a shift towards more positive oxidation potentials of the [Ru(bipy)$_2$(CN)$_2$] moiety, making it attractive for photoredox catalysis[1]. The effect was attributed to the concerted stabilization of metal-centered t_{2g} orbitals and a less pronounced effect on the bipy π* orbitals. On the other hand, the similar behavior of **RuEr** and the parent **Ru** complex both in acetonitrile solution and in the solid state, where no solvent dynamic

interactions are possible, points out that the main origin of the hypsochromic shift is herein solely related to the stabilization of the HOMO, which is not a purely metal-centered t_{2g} orbital, but has a significant contribution from the π orbitals of the CN^- group. The fact that CN^- groups have a much more relevant role in determining the emissive spectral features of **RuEr** over the bipy ligands, can find more support when observing the spectral shape of the emission band, which displays a shoulder at lower energies. Such "double band" feature is typically attributed in the literature to slow solvent reorganization effects[42], affecting the energies of the peripheral ligands' orbitals. However, in the case of **RuEr**, this interpretation cannot be taken into consideration as a similar feature is also observed in the solid state. Rather, the DFT-calculated MOs in Figure 4 and Table S3 evidence the different charge density distribution on the two asymmetrical bridging and non-bridging cyanide groups, giving rise to two sets of closely spaced HOMOs (Table S3) which may be accounted for to explain the observed spectral shape. On the other hand, peripheral bipy ligands are indeed accountable for crystalline state effects, which are nonetheless of high relevance for practical applications, since solid-state chemical sensors are desirable over solution-working systems[39]. In fact, the emission peak in the visible range is noticeably red-shifted in the solid state with respect to the solution, to a larger extent for **RuEr** than **Ru**. Typically, it can be expected that

the observed spectral differences in solution originate from solvent effects influencing the peripheral (bipy) ligands' orbitals (LUMOs)[39]. However, ruling out the role of the solvent, as previously pointed out, and considering the agreement of the observed PL red-shift with the absorption and DR spectra as above discussed, we may reliably infer that this phenomenon is related to intermolecular π-stacking interactions (or hydrogen-bonding) established in the solid state (Figure S3)[43].

Beyond the described peculiar emission chromism, a remarkable increase of the emission quantum yield of **RuEr** in the visible range up to 9.8% with respect to the 0.9% value of **Ru** is observed, resulting in a much brighter orange-red emission for the heterometallic assembly both in solution and in the solid state, as evidenced in the photographs of Figure 5c. This performance is contrary to that observed in the borylated analogs[1], where the decreased quantum yield with respect to the parent $[Ru(bipy)_2(CN)_2]$ moiety was ascribed to the influence of hydrogen-bonding or borylation in stabilizing both t_{2g} and e_g-like orbitals. The resulting relative lowering of the non-emissive metal-centered ^{3}MC states with respect to the emissive ^{3}MLCT, would cause quenching by favoring internal conversion and subsequent thermal deactivation. Instead, in the case of **RuEr**, DFT calculations indicate that the stabilization effect related to the coordination of the cyanide

ligand to Er(III) acts both on MLCT (or MLL'CT) as well as on MC (ligand contaminated) states. In addition, e_g-like orbitals, which significantly contribute already to the LUMO+1 in **Ru**, are raised in energy in **RuEr**, resulting in an even larger energy increase of the ^{3}MC states with respect to the emissive ^{3}MLCT, partly suppressing the main deactivation channel of the emission (Figure 6). These observations can provide a reliable explanation of the origin of the observed notable increase in the quantum yield in **RuEr**, despite part of the absorbed energy is transferred to Er(III) (vide infra).

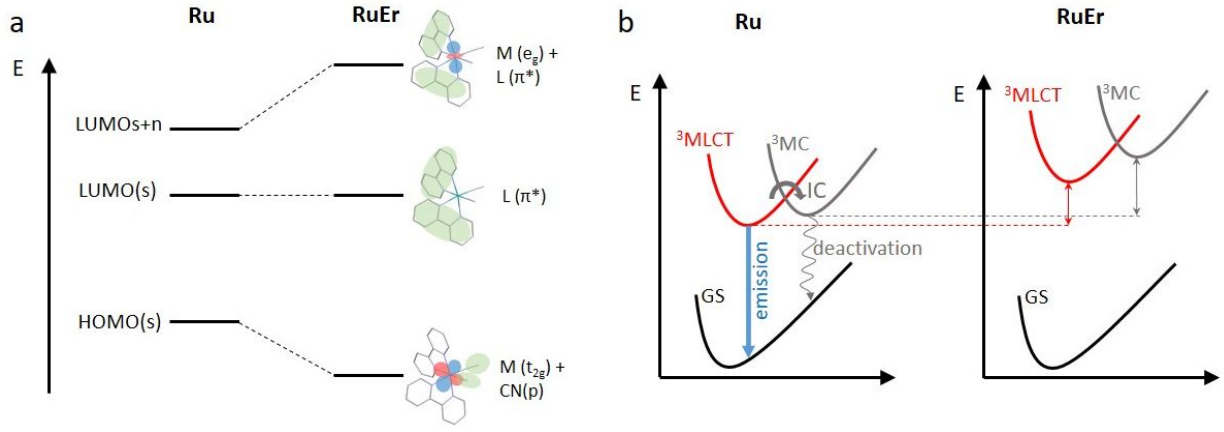

Figure 6. a) Simplified diagram of frontier MOs in **Ru** and **RuEr** highlighting the metal (M, blue and red shades), cyanide (CN^-) and bipy ligand (L) (green shades) orbitals contributions. b) Simplified scheme of the potential energy curves in **Ru** and **RuEr** together with emission and deactivation pathways (GS = ground state; IC = internal conversion).

NIR-range PL properties. Upon photoexcitation in the lowest absorption band, **RuEr** displays the characteristic Er(III)-centered emission peaked at 1530 nm (Figure 5d) and related to a 4*f* intrashell $^4I_{13/2} \rightarrow {}^4I_{15/2}$ transition. Therefore, similarly to the most investigated tetracyanideruthenate diimine Ru(II) derivatives, also $[Ru(bipy)_2(CN)_2]$ is revealed as an effective sensitizer to NIR-emissive lanthanide ions[10,12]. The sensitization process is believed to occur, as typically found in lanthanide complexes[44], through energy transfer from the triplet excited states of the antenna moiety to the upper energy levels of Er(III), and in this heterometallic assembly it reliably involves the Ru(II)-centered ^{3}MLCT states. This mechanism is confirmed by the fact that in **RuEr** approximately the same emission intensity is observed in degassed and air-equilibrated (dashed line in Figure 5a) solution, as opposed to the behavior displayed by **Ru**, where phosphorescence (triplet) quenching can be attributed to molecular oxygen[45]. Such observation points out that in **RuEr** excited triplet depopulation caused by energy transfer to the Er(III) ion is kinetically competitive with oxygen quenching, thus accounting for the relatively efficient sensitization of the NIR emission. Although the antenna mechanism in this heterometallic compound is far from reaching the efficiency, close to 100%, observed in some mononuclear erbium complexes[44], it also allows for dual Vis-NIR emission to be stimulated under single-wavelength excitation. The spectral shape of the emission

band mirrors the observed absorption features and is characteristic of the specific coordination environment of the Er(III) ion (Figure S4). Noticeably, the integrated spectral area and FWHM (full width at half maximum) is considerably smaller, by at least 15%, with respect to ome archetypical erbium complexes with 8-hydroquinolines[46] [47]and chlorocyananilate ligands[48] (Figure S5 and Table S6). We may suppose that this peculiarity, which is a favored condition to realize nonlinear or single photon emission, originates from a weak crystal field induced by the monodentate bridging CN^- group from the neutral Ru(II) metalloligand in comparison with negatively charged oxygen donor ligands[49]. Despite Er(III) emission is likely significantly quenched by vibrational de-excitation via water molecules and possibly CH groups[14], as evidenced in Figures 3d and S4, it is however worth underlining that the reported example represents, to the best of our knowledge, the first clearly detectable and well-defined emission spectrum of Er(III) in heterometallic Ru(II)-Er(III) systems. We may tentatively ascribe this result not only to the significant distance (>5Å) of Er(III) from quenching CH oscillators in the **RuEr** assembly, but also to the lowered number of cyanide groups, as potential additional quenchers of the $[Ru(bipy)_2(CN_2)]$ moiety, with respect to the more popular tetracyanoruthenate(II) derivatives[18]. Further investigations on the mechanisms and efficiency of lanthanide sensitization by time-

resolved and ultra-fast transient absorption studies as well as on the dynamics of NIR emission are currently being carried out in our laboratories to further elucidate the interesting dual photoluminescence properties of this and analogous compounds with other lanthanide ions. We can reliably infer that the replacement of the two water molecules coordinated in *cis* configuration to the lanthanide ion, can result in a significant improvement of the emission properties in the NIR, opening novel perspectives for the further development of such dual Vis-NIR luminescent systems.

4. CONCLUSIONS

In this work we have presented the synthesis, crystal structure, and an in-depth investigation of the optical and emissive properties of a unique heterometallic cyanide-bridged *d-f* assembly combining Er(III) and the $[Ru(bipy)_2(CN)_2]$ complex-as-ligand and showing intense dual emission in the visible and NIR ranges. The design strategy based on the use of the neutral biscyanoruthenium (II) metalloligand allows for accommodating inorganic anions such as nitrate and oxalate for the completion of the coordination sphere of the lanthanide ion, thus reducing the available sites for the direct bonding of water molecules or other NIR-emission quenchers-containing ligands in comparison to the most popular tetracyanoruthenate(II) derivatives. As a result, the crystal structure of the obtained mixed Ru(II)-Er(III) complex consists of a dimeric

tetranuclear architecture where two Ru-CN-Er monomeric units are connected by an oxalate ion bridging two Er(III) in a bis-bidentate fashion. Strikingly, the so-obtained heterometallic assembly, not only shows a notable hypsochromic shift of both the absorption and emission spectral features in the visible range, but also a remarkable tenfold increase of the emission quantum yield. With the support of DFT calculations, we demonstrate that this behavior mainly originates from the stabilization of the HOMO, which has a mixed Ru(II)(*d*)/CN(p) character, thanks to the electron-withdrawing effect and strong bonding to Er(III). At the same time, the e_g-like orbitals of Ru(II) in the octahedral field are raised in energy, determining a widened gap and decreased overlap between the emissive ^{3}MLCT (or ^{3}MLL'CT) state and the non-emissive ^{3}MC state, thus accounting for the suppression of the main thermal deactivation channel and the resulting increased emission of the *d-f* mixed-metal assembly with respect to the parent Ru(II) complex. Furthermore, it is demonstrated that the $[Ru(bipy)_2(CN)_2]$ metalloligand acts as a relatively efficient antenna towards Er(III). Thanks to the reduced number of quenching water molecules, CH and CN groups in the surroundings of the lanthanide ion, it has been possible to retrieve well detectable and defined Er(III) sensitized photoluminescence, whereas room for improvement of the NIR emission performance is identified by synthetic design. As a final consideration, we point out that

$[Ru(bipy)_2(CN)_2]$ is a powerful ionochromic "turn on" luminescent sensor in the visible range toward lanthanide ions, thanks to the pivotal role of the cyanide groups in tuning the energy levels and even enhancing the emission intensity upon coordination. In this context, it is worth noting that the designed mixed Ru(II)-Er(III) assembly bears one bridging and one "free" cyanide group which could in principle act as further sensing unit. This observation highlights the promising potential of such *d-f* assembly for various applications, not only as dual emitter but also for chemical luminescence sensing.

ASSOCIATED CONTENT

Supporting Information

Supporting Information include: additional crystallographic figures; FT-IR spectra and related discussion; DFT-calculated frontiers MOs; TD-DFT data; additional PL data in the NIR region.

Accession Codes

CCDC 2327288 contains the supplementary crystallographic data for this paper. These data can be obtained free of charge via www.ccdc.cam.ac.uk/data_-request/cif, or by emailing

data_request@ccdc.cam.ac.uk, or by contacting The Cambridge Crystallographic Data Centre, 12 Union Road, Cambridge CB21EZ, U.K.; fax: +44 1223336033

AUTHOR INFORMATION

Corresponding Authors

*Flavia Artizzu – orcid.org/0000-0003-3773-2806 Email: flavia.artizzu@uniupo.it.

* Luca Pilia – orcid.org/0000-0001-8753-7094 Email: luca.pilia@unica.it

Author Contributions

The manuscript was written through contributions of all authors. All authors have given approval to the final version of the manuscript.

Funding Sources

This work received support from the European Innovation Council under the Horizon Europe framework programme through a HORIZON-EIC-2022-PATHFINDERCHALLENGES-01-06 project "ARTEMIS – *Molecular Materials for on-chip integrated quantum light sources*" – GA n. 101115149.

We also acknowledge financial support under the National Recovery and Resilience Plan (NRRP), Mission 4, Component 2, Investment 1.1, Call for tender No. 104 published on 2.2.2022 by the Italian Ministry of University and Research (MUR), funded by the European Union – Next Generation EU– Project Title "QuantaMol - *Molecular Quantum Light Sources"* – CUP C53D23007330001- Grant Assignment Decree No. 1380 adopted on 01-09-2023 by the Italian Ministry of University and Research (MUR).

ACKNOWLEDGMENT

F.A., L.P. and D.M. gratefully acknowledge the European Innovation Council for financial support through the EIC Pathfinder project "ARTEMIS" G. A. n. 101115149. F.A. and L.P. are also grateful to the Italian Ministry of University and Research (MUR) for financial support through the PRIN 2022 PNRR project "QuantaMol" CUP C53D23007330001, funded by the European Union – Next Generation EU. F.A. gratefully acknowledges FWO (Research Foundation Flanders) for a Travel Grant (ID V506423N). Z.W.C. acknowledges the China Scholarship Council (CSC, Project 202206750007) and Gent BOF (BOF.CHN.2022.0008.01) for financial support. Prof. Francesca Mocci (University of Cagliari, Italy) is acknowledged for providing access to computational facilities.

REFERENCES

[1] Schmid, L.; Kerzig, C.; Prescimone, A.; Wenger, O. S. Photostable Ruthenium(II) Isocyanoborato Luminophores and Their Use in Energy Transfer and Photoredox Catalysis *JACS Au* **2021**, *1* (6), 819-832.

[2] Ji, S.; wu, W.; Wu, W.; Song, P.; Han, K.; Wang, Z.; Liu, S.; Guo, H.; Zhao, J. Tuning the luminescence lifetimes of ruthenium(II) polypyridine complexes and its application in luminescent oxygen sensing *J. Mater. Chem.*, **2010**, *20*, 1953–1963.

[3] Tomar, N.; Agrawal, A.; Dhaka, V. S.; Surolia, P. K. Ruthenium complexes based dye sensitized solar cells: Fundamentals and research trends *Solar Energy* **2020**, *207*, 59–76

[4] Elgar, C. E.; Yusoh, N. A.; Tiley, P. R.; Kolozsvári, N.; Bennet, L. G.; gamble, A.; Péan, E. V.; Davies, M. L.; Staples, C. J.; Ahmad, H.; Gill, M. R. Ruthenium(II) Polypyridyl Complexes as FRET Donors: Structure- and Sequence-Selective DNA-Binding and Anticancer Properties *J. Am. Chem. Soc.* **2023**, *145*, 2, 1236-1246.

[5] Strieth-Kalthoff, F.; Glorious, F. Triplet Energy Transfer Photocatalysis: Unlocking the Next Level *Chem*, **2020**, *6*, 1888-1903.

[6] Knighton, R. C.; Beames, J. M.; Pope, S. J. A. Polycationic Ru(II) Luminophores:Syntheses, Photophysics, and Application in Electrostatically Driven Sensitization of Lanthanide Luminescence *Inorg. Chem.* 2023, *62*, 19446−19456.

[7] Kitamura, N.; Sato, M.; Kim, H.-B.; Obata, R.; Tazuke, S. Solvatochromism in the Excited State of the cis-Dicyanobis(1,10-phenanthroline)ruthenium(II) Complex *Inorg. Chem.* **1988**, *27*, 651-658.

[8] Feng, H.; Zhang, F.; Lai, S.-W.; Yiu, S.-M.; Ko, C.-C. Luminescent Cyanoruthenate(II)-Diimine and Cyanoruthenium(II)-Diimine Complexes *Chem. Eur. J.* **2013**, *19*, 15190 – 15198.

[9] Abe, T.; Suzuki, T.; Shinozaki, K. Luminescence Change by the Solvent of Crystallization, Solvent Reorganization, and Vapochromism of Neutral Dicyanoruthenium(II) Complex in the Solid State *Inorg. Chem.* **2010**, *49*, 1794–1800.

[10] Miller, T. A.; Jeffery, J. C.; Ward, M. D.; Adams, H.; Pope, S. J. A.; Faulkner, S. Photoinduced Ru–Yb energy transfer and sensitised near-IR luminescence in a coordination polymer containing co-crystallised $[Ru(bipy)(CN)_4]^{2-}$ and Yb(III) units *Dalton Trans.*, **2004**, 1524-1526.

[11] Adams, H.; Alsindi, W. Z.; Davies, G. M.; Duriska, M. B.; Easun, T. L.; Fenton, H. E.; Herrera, J.-M.; George, M. W.; Ronayne, K. L.; Sun, X.-Z.; Towrie, M.; Ward, M. D. New members of the $[Ru(diimine)(CN)_4]^{2-}$ family: structural, electrochemical and photophysical properties *Dalton Trans.*, **2006**, 39–50.

[12] Ward, M. D. Transition-metal sensitised near-infrared luminescence from lanthanides in d–f heteronuclear arrays *Coord. Chem. Rev.* **2007**, *251*, 1663-1677.

[13] Kostin, G. A.; Borodin, A. O.; Kuratieva, N. V.; Bogomyakov, A. S.; Mikhailov, A. A. Tetranuclear Ru_2Ln_2 complexes of heavier lanthanides (Gd, Tb, Dy, Ho, Lu) with $[RuNO(NO_2)_4OH]^{2-}$ anion, combining SMM properties and photoswitchable Ru-NO group, Inorg. Chim. Acta, 2018, 479, 135-140.

[14] Mara, D.; Artizzu, F.; Smet, P. F.; Kaczmarek, A. M.; Van Hecke, K.; Van Deun, R. **Vibrational** Quenching in Near-Infrared Emitting Lanthanide Complexes: A Quantitative Experimental Study and Novel Insights *Chem. Eur. J.* **2019**, 25, 15944-15956.

[15] Chow, C.-F.; Kong, H.-K.; Leung, S.-W.; Chiu, B.K.W.; Koo, C.-K.; Lei, E.N.Y.; Lam, M.H.W.; Wong, W.-T.; Wong, W.-Y. Heterobimetallic Ru(II)–Eu(III) Complex as Chemodosimeter for Selective Biogenic Amine Odorants Detection in Fish Sample *Anal. Chem.* **2011**, *83*, 289–296.

[16] Chow, C.-F.; Lam, M.H.W.; Wong, W.-Y. Design and Synthesis of Heterobimetallic Ru(II)–Ln(III) Complexes as Chemodosimetric Ensembles for the Detection of Biogenic Amine Odorants *Anal. Chem*. **2013**, *85*, 8246–8253.

[17] Chorazy, S.; Wyczesany, M.; Sielucka, B. Lanthanide Photoluminescence in Heterometallic Polycyanidometallate-Based Coordination Networks *Molecules* **2017**, *22*, 1902.

[18] Baca, S. G.; Adams, H.; Sykes, D.; Faulkner, S.; Ward, M. D. Three-component coordination networks based on $[Ru(phen)(CN)_4]^{2-}$ anions, near-infrared luminescent lanthanide(III) cations, and ancillary oligopyridine ligands: structures and photophysical properties *Dalton Trans.*, **2007**, 2419–2430.

[19] Liu, C. F.; Liu, N. C.; Bailar, J. C. Jr. A specific Synthesis for Bis(bipyridine)ruthenium Compounds *Inorg. Chem.,* **1964**, *3***,** 1197-1198

[20] Demas, J. N.; Turner, T. F.; Crosby, G. A. Preparation and Thin-Layer Chromatography of cis-Dicyanobis(2,2'-bipyridine)ruthenium(II) *Inorg. Chem.* **1969**, *8*, 674-675.

[21] Bruker (2012). APEXII. Bruker AXS Inc., Madison, Wisconsin, USA.

[22] Krause, L., Herbst-Irmer, R., Sheldrick G.M. & Stalke D., Comparison of silver and molybdenum microfocus X-ray sources for single-crystal structure determination *J. Appl. Cryst.* **2015**, 48 3-10.

[23] Sheldrick, G. M. Crystal structure refinement with SHELXL *Acta Crystallogr. Sect. A Found. Crystallogr.*, **2015**, 71, 3–8

[24] Dolomanov, O. V.; Bourhis, L. J.; Gildea, R. J.; K. Howard J. A.; Puschmann H. *OLEX2*: a complete structure solution, refinement and analysis program *J. Appl. Crystallogr*. **2009**, 42, 339–341.

[25] Parr, R.G.; Yang, W. Density Functional Theory of Atoms and Molecules; Oxford University Press: Oxford, UK, 1989.

[26] Frisch, M.J.; Trucks, G.W.; Schlegel, H.B.; Scuseria, G.E.; Robb, M.A.; Cheeseman, J.R.; Scalmani, G.; Barone, V.; Petersson, G.A.; Nakatsuji, H.; et al. Gaussian 16, Revision C.01, Gaussian, Inc.: Wallingford, CT, USA, **2016**.

[27] Yanai, T.; Tew, D.; Handy, N. A new hybrid exchange–correlation functional using the Coulomb-attenuating method (CAM-B3LYP). *Chem. Phys. Lett.* 2004, *393*, 51–57.

[28] Petersson, G.A.; Bennett, A.; Tensfeldt, T.G.; Al-Laham, M.A.; Shirley, W.A.; Mantzaris, J. A complete basis set model chemistry. I. The total energies of closed-shell atoms and hydrides of the first-row elements. *J. Chem. Phys.* **1988**, *89*, 2193–2218.

[29] Hay, P.J.; Wadt, W.R. Ab initio effective core potentials for molecular calculations. Potentials for K to Au including the outermost core orbitals. *J. Chem. Phys.* **1985**, *82*, 299–310.

[30] Andrae, D.; Haussermann, U.; Dolg, M.; Stoll, H.; Preuss, H. Energy-adjusted ab initio pseudopotentials for the second and third row transition elements. *Theor. Chim. Acta* **1990**, *77*, 123–141.

[31] Scalmani, G.; Frisch, M. J.; Mennucci, B.; Tomasi, J.; Cammi, R.; Barone, V. Geometries and properties of excited states in the gas phase and in solution: Theory and application of a time-dependent density functional theory polarizable continuum model *J. Chem. Phys.*, **2006**, *124* 094107.

[32] Cossi, M.; Rega, N.; Scalmani, G.; Barone, V. Energies, structures, and electronic properties of molecules in solution with the C-PCM solvation model *J. Comp. Chem.*, **2003**, *24*, 669-681.

[33] Thompson, M. A. ArgusLab 4.0.1, Planaria Software LLC: Seattle, WA, USA, 2021. Available online: http://www.arguslab.com/arguslab.com/ArgusLab.html/.

[34] O'Boyle, N. M.; Tenderholt, A. L.; Langner, K. M cclib: A library for package-independent computational chemistry algorithms *J. Comp. Chem.*, 2008, *29*, 839-845.

[35] Schilt, A. A. Proton Affinities of Some Cyanide and Aromatic Diimine Complexes of Iron, Ruthenium and Osmium *J. Am. Chem. Soc.,* **1963***,* 85, 904-908.

[36] Odongo, O. S.; Endicott, J. F.; Heeg, M. J. CSD Communication (Private Communication) 2006, CCDC 613874.

[37] Artizzu, F.; Pilia, L.; Serpe, A.; Mara, D.; Casula, M. F.; Marchiò, L.; Deplano, P. Anion-Induced Structural Diversity and Optical Chromism in a Series of Cyano-Bridged Heterometallic 3d-4f Coordination Polymers *Molecules* **2023**, *28*, 2871.

[38] Atzori, M; Artizzu, Functional Molecular Materials: An Introductory Textbook (1st ed.). **2018**, Jenny Stanford Publishing. https://doi.org/10.1201/9781351233668. Chapter 3 and references therein.

[39] Abe, T.; Suzuki, T.; Shinozaki, K. Luminescence Change by the Solvent of Crystallization, Solvent Reorganization, and Vapochromism of Neutral Dicyanoruthenium(II) Complex in the Solid State *Inorg. Chem.* **2010**, *49*, 1794–1800.

[40] Yang, C.; Artizzu, F.; Folens, K.; Du Laing, G.; Van Deun, R. Excitation dependent multicolour luminescence and colour blueshifted afterglow at room-temperature of europium incorporated hydrogen-bonded multicomponent frameworks *J. Mater. Chem. C*, **2021**, *9*, 7154-7152.

[41] It is noted that for both $[Ru(bipy)_2(CN)_2]$ and **RuEr**, a set of closely spaced MOs of similar orbital density distribution as the HOMO and LUMO represented in Figure 4 is found (Tables S1-S3). Therefore the most correct interpretation of HOMO and LUMO orbitals should refer to the whole set of closely spaced orbitals and not to single ones. Furthermore, the dimeric nature of **RuEr** results in doubly degenerate MOs.

[42] Kitamura, N.; Kim, H.-B.; Kawanishi, Y. Obata, R.; Tazuke, S. Time-Resolved Emission Spectra of $Ru(bpy)_3Cl_2$ and cis-$Ru(bpy)_2(CN)_2$ at Low Temperature *J. Phys. Chem.* **1986**, *90*, 1488-1491.

[43] Mara, D.; Pilia, L.; Van de Steen, M.; Miletto, I.; Zeng, M.; Van Hecke, K.; Serpe, A.; Deplano, P.; Van Deun, R.; Artizzu, F. Single-component panchromatic white light generation, and tuneable excimer-like visible orange and NIR emission in a Dy quinolinolate complex *J. Mater. Chem. C*, **2021**, *9*, 15641-15648.

[44] Artizzu, F.; Quochi, F.; Marchiò, L.; Figus, C.; Loche, D. Atzori, M.; Sarritzu, V.; Kaczmarek, A. M.; Van Deun, R.; Saba, M.; Serpe, A.; Mura, A.; Mercuri, M. L.; Bongiovanni, G.; Deplano, P. Light Conversion Control in NIR-Emissive Optical Materials based on Heterolanthanide Er_xYb_{3-x} Quinolinolato Molecular Components *Chem. Mater.*, **2015**, *27*, 4082–4092.

[45] Morris, K. J.; Roach, M. S.; Xu, W.; Demas, J. N. DeGraff, B. A. Luminescence Lifetime Standards for the Nanosecond to Microsecond Range and Oxygen Quenching of Ruthenium(II) Complexes *Anal. Chem.* **2007**, *79*, 9310-9314.

[46] Artizzu, F.; Deplano, P.; Marchiò, L.; Mercuri, M. L.; Pilia, L.; Serpe, A.; Quochi, F.; Orrù, R.; Cordella, F.; Saba, M.; Mura, A.; Bongiovanni, G. New Insights on Near-Infrared Emitters Based on Er-quinolinolate Complexes: Synthesis, Characterisation, Structural and Photophysical Properties; *Adv. Funct. Mater.* **2007,** *17*, 2365-2376.

[47] Artizzu, F.; Deplano, P.; Marchiò, L.; Mercuri, M. L.; Pilia, L.; Serpe, A.; Quochi, F.; Orrù, R.; Cordella, F.; Meinardi, F.; Tubino, R.; Mura, A.; Bongiovanni, G. Structure and emission properties of Er_3Q_9 (Q = 8-quinolinolate); *Inorg. Chem.* **2005**; *44*; 840-842.

[48] Artizzu, F.; Atzori, M.; Liu, J.; Mara, D.; Van Hecke, K.; Van Deun R. Solution-processable Yb/Er 2D-layered metallorganic frameworks with high NIR-emission quantum yields *J. Mater. Chem. C*, **2019**, *7*, 11207-11214.

[49] Golesorkhi, B.; Nozary, H.; Fürstenberg, A.; Piguet, C. Erbium complexes as pioneers for implementing linear light-upconversion in molecules *Mater. Horiz.*, **2020**, *7*, 1279-1296.

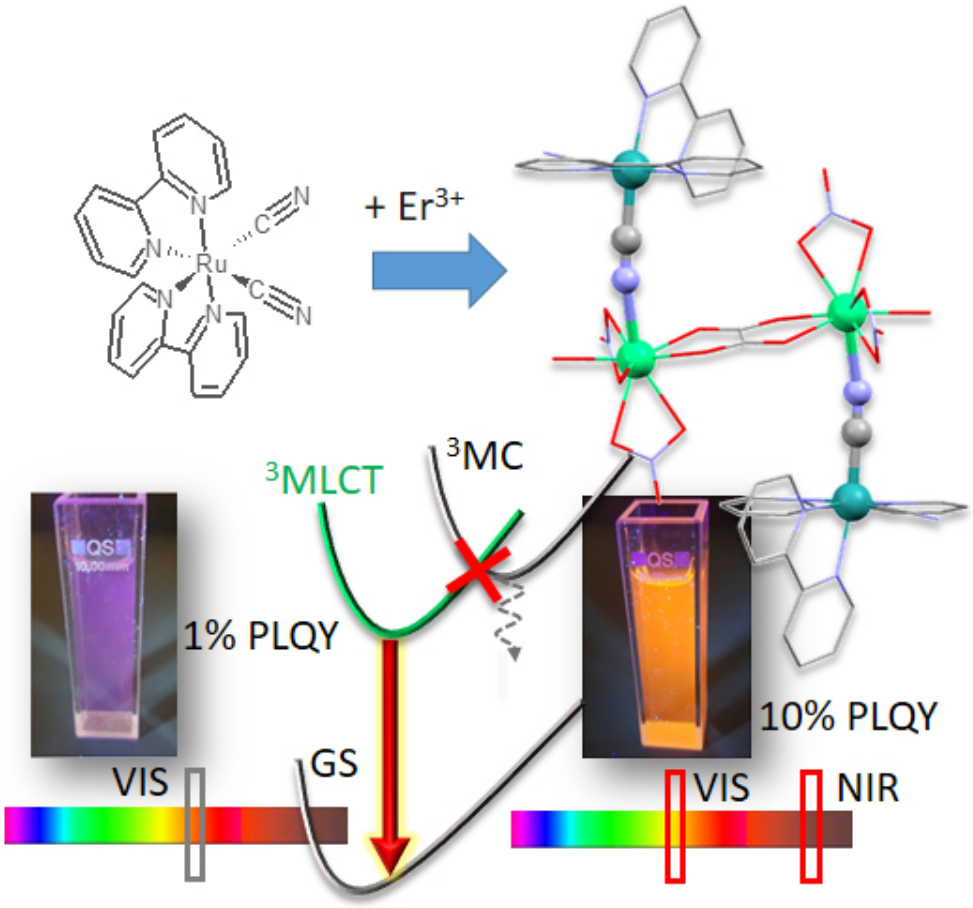

141x129mm (96 x 96 DPI)